Letter

A High-Performance and Long-Lived Cu/SiO2 Nanocatalyst for CO2 Hydrogenation

Zhi-Qiao Wang, Zhong-Ning Xu, Si-Yan Peng, Ming-Jian Zhang, Gang Lu, Qing-Song Chen, Yumin Chen, and Guo-Cong Guo

ACS Catal., **Just Accepted Manuscript** • DOI: 10.1021/acscatal.5b00682 • Publication Date (Web): 08 Jun 2015

A High-Performance and Long-Lived Cu/SiO_2 Nanocatalyst for CO_2 Hydrogenation

Zhi-Qiao Wang,[†,‡] Zhong-Ning Xu,[*,†,‡] Si-Yan Peng,[†] Ming-Jian Zhang,[†] Gang Lu,[†] Qing-Song Chen,[†] Yumin Chen,[†] and Guo-Cong Guo[*,†]

[†]State Key Laboratory of Structural Chemistry, Fujian Institute of Research on the Structure of Matter, Chinese Academy of Sciences, Fuzhou, Fujian 350002, P. R. China

[‡]Key Laboratory of Coal to Ethylene Glycol and Its Related Technology, Chinese Academy of Sciences, Fuzhou, Fujian 350002, P. R. China

Abstract: Cu-based nanocatalysts have been widely used for CO2 hydrogenation, but the poor stability is the bottleneck for further industrial application. A high-performance and long-lived Cu/SiO_2 nanocatalyst was synthesized by ammonia-evaporation method for CO_2 hydrogenation. The conversion of CO_2 reaches up to 28%, which is close to the equilibrium conversion of CO_2 (30%), and the selectivity to methanol is 21.3%, which is much higher than the equilibrium selectivity (6.9%) at 320 °C and 3.0 MPa. Furthermore, after 120 h evaluation the conversion can still maintain at a high value (27%), which is much better than Cu/SiO_2 catalyst prepared by traditional impregnation. The Cu^+ species has been demonstrated to be the active component for the activation and conversion of CO_2. The higher ratio of $Cu^+/(Cu^0 + Cu^+)$ and interaction between metal and support deriving from copper phyllosilicate are mainly responsible for the high catalytic activity and excellent stability, respectively.

Keywords: *ammonia-evaporation method, Cu/SiO_2 nanocatalyst, CO_2 hydrogenation, copper phyllosilicate, Cu^+ species*

CO_2 is a main kind of "greenhouse gas", which is produced by the utilization of carbon-rich fossil fuels (e.g., coal, oil and natural gas).[1,2] In recent decades, the rapidly raising concentration of CO_2 in the atmosphere results in a series of environment problems, such as global warming, ocean acidification, climate change and so on.[3-5] Though the natural photosynthesis can convert CO_2 to organic carbon, it is far from enough to consume so much CO_2 in a short period with its increasing concentration.[6] Recently, much attention has been attracted to the catalytic conversion of CO_2 because it can not only close the anthropogenic carbon cycle but also provide useful chemicals such as epoxides, methanol, formic acid and so on.[7-13] However, few industrial processes have utilized CO_2 as a raw material to produce high-value chemicals.[14] The biggest challenge is that CO_2 activating requires a large number of energy due to its high oxidation state and thermodynamic stability under lacking of effective catalysts.[15,16] Hence, it is quite essential to develop high-performance catalysts to activate and convert CO_2 under mild conditions.[17,18]

Cu-based nanocatalysts have been widely used in the field of CO_2 hydrogenation because of their high activity for activation and conversion of CO_2.[19-27] The catalytic activity of Cu-based nanocatalyst would dramatically improve with decreasing of the Cu particle size.[28] However, Cu-based nanocatalysts are not stable because Cu nanoparticles (NPs) would easily aggregate and sinter during the preparation and using processes.[29] Notably, the growth of metal NPs, which can result in losing of active surface area, is the main reason for deactivation of many supported nanocatalysts.[29] The poor stability of Cu NPs is the bottleneck for industrial application.[30, 31] Introducing structure promoters has been used to mitigate the growth Cu NPs[32, 33], but sometimes it just does not work because it would restrict the chemical composition and functionality of Cu-based nanocatalysts.[29, 34, 35] Hence, developing a new strategy to prepare high-performance and long-lived supported Cu-based nanocatalysts without any promoter has important significance for activation and conversion of CO_2.

In this work, a high-performance and long-lived Cu/SiO_2 nanocatalyst (denoted as Cu/SiO_2-AE, see the preparation process details in ESI) has been synthesized by ammonia-evaporation (AE) method.[36] CO_2 hydrogenation to methanol was chosen as a probe reaction to evaluate the Cu/SiO_2-AE nanocatalyst.

Figure 1 presents the performances of Cu/SiO_2-AE nanocatalyst for CO_2 hydrogenation to methanol. The products of Cu/SiO_2-AE nanocatalyst for CO_2 hydrogenation are methanol, CO and a small amount of methane.

With the reaction temperature increasing from 260 to 380 °C, the conversion of CO_2 increases from 8.2 to 35.0% and the selectivity to methanol decreases from 40.2% to 5.9%, implying low temperature is suitable for the synthe-

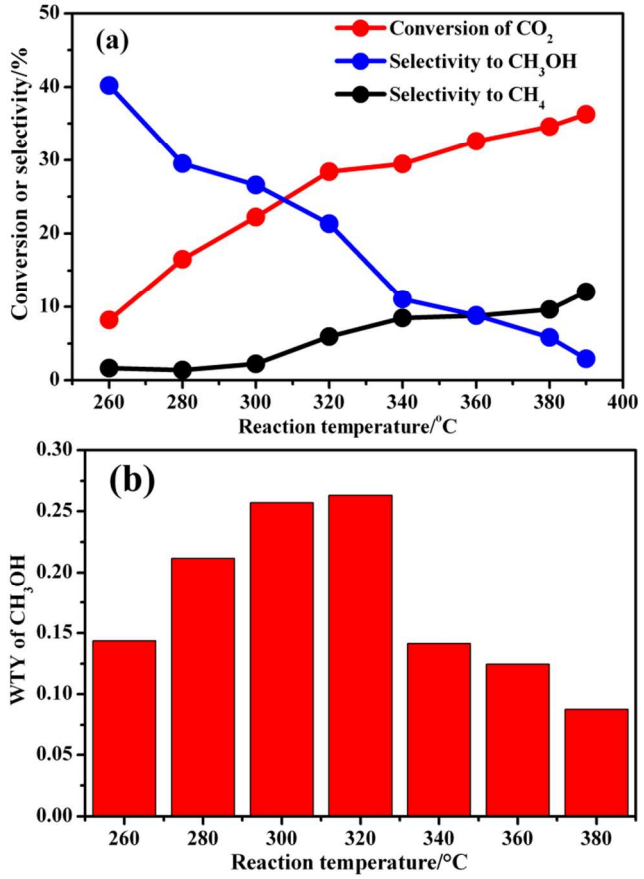

Figure 1. The performances of Cu/SiO_2-AE nanocatalyst for CO_2 hydrogenation[i]: (a) Conversion of CO_2, selectivity to CH_3OH and selectivity to CH_4 as functions of reaction temperature, (b) WTY[ii] of methanol as functions of reaction temperature. [i] Reaction conditions: 0.3 g catalyst, 3.0 MPa, weight hour space velocity (WHSV) = 16 $L{\cdot}g_{cat}^{-1}{\cdot}h^{-1}$, $H_2 : CO_2$ = 4 : 1. [ii] WTY represents the weight-time yield, grams of methanol per gram of catalyst per hour ($g{\cdot}g_{cat.}^{-1}{\cdot}h^{-1}$).

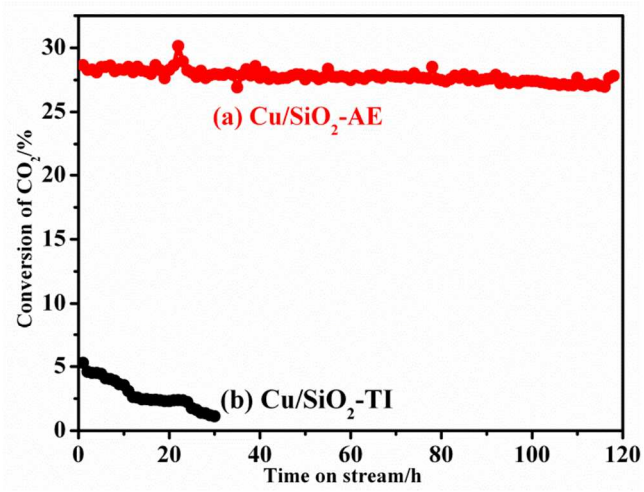

Figure 2. Conversion of CO_2 as functions of time on stream at 320 °C and 3.0 MPa over (a) Cu/SiO_2-AE and (b) Cu/SiO_2-TI nanocatalysts.

sis of methanol but not for the CO_2 catalytic conversion[37] (Figure 1a). The conversion of CO_2 at 320 °C is close to the equilibrium conversion (30%, Table S1), suggesting the as-synthesized Cu/SiO_2-AE nanocatalyst is of high activity for CO_2 hydrogenation. Interestingly, the selectivity to methanol at 320 °C is 21.3%, which is much higher than that (6.9%) of equilibrium selectivity to methanol (Figure S1). The main product CO can further hydrogenated to methanol over Cu/SiO_2-AE nanocatlayst (Figure S2). The influence of WHSV has been presented in Figure S3. The weight time yield (WTY) of methanol presents the volcanic type trend and reaches the maximum of 0.26 $g{\cdot}g_{cat.}^{-1}{\cdot}h^{-1}$ at 320 °C according to the conversion and selectivity (Figure 1b). Most importantly, the conversion of CO_2 over Cu/SiO_2-AE nanocatalyst can still maintain at a high value (27%) after 120 h evaluation (Figure 2), which indicates that the as-synthesized Cu/SiO_2-AE nanocatalyst is quite stable and has promising industrial application value. In order to highlight the advantage of ammonia-evaporation method, a Cu/SiO_2 nanocatalyst had been synthesized by traditional impregnation method for comparison (denoted as Cu/SiO_2-TI, see the preparation process details in ESI). The catalytic activity of Cu/SiO_2-TI nanocatalyst is just 5% at 320 °C, which is much less than that of Cu/SiO_2-AE nanocatalyst (Figure S4) under the same reaction conditions. Furthermore, the stability of Cu/SiO_2-TI nanocatalyst is quite poor since the catalytic activity is almost completely lost after 25 h (Figure 2). Moreover, the turnover frequency (TOF) values (details shown in ESI) of Cu/SiO_2-AE and Cu/SiO_2-TI nanocatalysts are 79.85 and 10.44 h^{-1}, respectively. The intrinsic TOF value of Cu/SiO_2-AE nanocatalyst is 7.7 times as much as that of Cu/SiO_2-TI nanocatalyst, indicating that the Cu/SiO_2-AE nanocatalyst is a high-performance catalyst for CO_2 hydrogenation.

The powder X-ray diffraction (PXRD) patterns of calcined Cu/SiO_2-AE samples reveal that the main peaks centred at 2θ = 30.8, 35.0, 57.5, 62.3 ° (JCPDS No. 027–0188, Figure 3a), which can be indexed to the phase of copper phyllosilicate.[29] Meanwhile, there is the phase of CuO (2θ = 32.2, 35.2, 38.4, 48.4, 53.2, 58.0, 61.2, 65.9, 67.7 °) (JCPDS No. 044–0706, Figure 3b) in calcined Cu/SiO_2-TI sample.[26] The board peaks at 22 ° belong to the amorphous SiO_2 support (Figure 3).[26] Fourier-transform IR (FT-IR) spectra were further measured to discriminate Cu species. There are two shoulder peaks at 1040 and 670 cm^{-1} in calcined Cu/SiO_2-AE sample (Figure S5a), confirming the existing of copper phyllosilicate.[38] There were no corresponding shoulder peaks in the FT-IR spectroscopy of calcined Cu/SiO_2-TI sample (Figure S5b), suggesting that there was no copper phyllosilicate in the Cu/SiO_2-TI sample.[38] Cu 2p X-ray photoelectron spectroscopy (XPS) spectra are shown in Figure 4. Cu $2p_{3/2}$ peak binding energy of calcined Cu/SiO_2-AE sample is 935.96 eV (Figure 4a), which is consistent with 936.0 eV of copper phyllosilicate. Meanwhile, Cu $2p_{3/2}$ peak binding energy of calcined Cu/SiO_2-TI sample is 933.75 eV (Figure 4b) corresponding to the 933.6 eV of CuO.[38] Based on the discussion above,

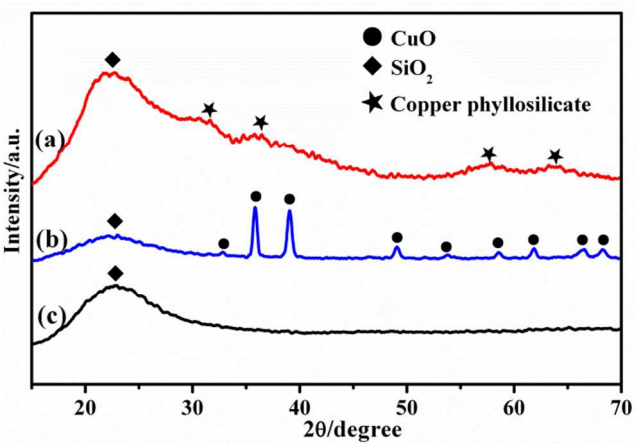

Figure 3. XRD patterns of (a) calcined Cu/SiO_2-AE sample, (b) calcined Cu/SiO_2-TI sample, and (c) $mSiO_2 \cdot nH_2O$.

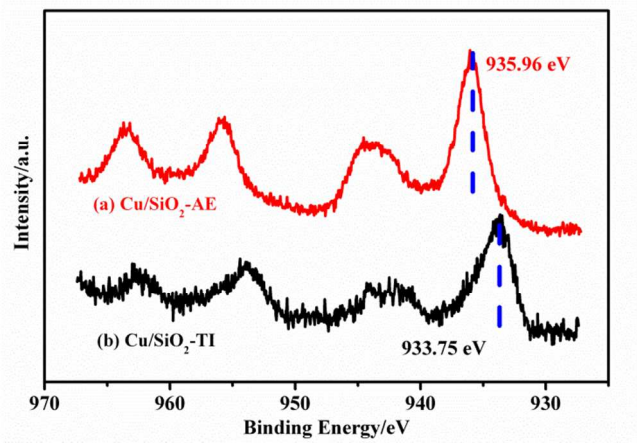

Figure 4. Cu 2p XPS spectra of calcined (a) Cu/SiO_2-AE and (b) Cu/SiO_2-TI samples.

we conclude that the main Cu species in calcined Cu/SiO_2-AE and Cu/SiO_2-TI samples are copper phyllosilicate and CuO, respectively. The Cu $2p_{3/2}$ peak binding energy shifts from 933.75 to 935.96 eV (Figure 4), demonstrating the existence of interaction between metal and support in calcined Cu/SiO_2-AE sample due to the formation of copper phyllosilicate (Figure S6 and S7).[39] The interaction was further proved by the combination of Si 2p XPS (Figure S8), H_2-TPR (Figure S9), PXRD (Figure S10), H_2-TGA (Figure S11) and UV-Vis-NIR diffuse reflectance spectroscopy (Figure S12) characterizations. The existence interaction can effectively restrain the migration and aggregation, which mainly accounts for the long life of Cu/SiO_2-AE nanocatalyst without any structure promoters.

The FT-IR in Figure S5b confirm that the disappearing of copper phyllosilicate in the freshly reduced Cu/SiO_2-AE. The PXRD pattern of freshly reduced Cu/SiO_2-TI nanocatalyst (Figure S13c) shows obvious diffraction peaks at 43.30, 50.44 and 74.10 °, which are assigned to Cu (111), (200) and (220) planes (JCPDS No. 070–3039), respectively. The average size of Cu NPs for Cu/SiO_2-TI nanocatalyst is about 46.5 nm, which is calculated by the Scherrer

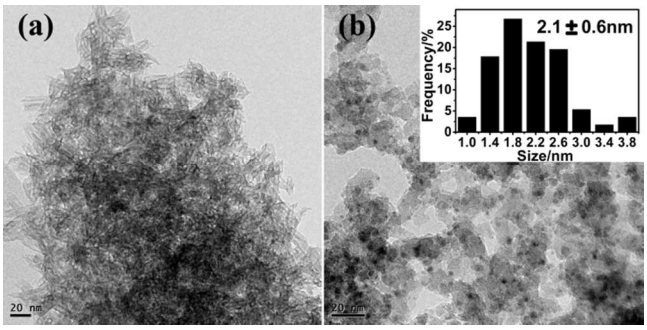

Figure 5. TEM images of (a) calcined Cu/SiO_2-AE sample and (b) freshly reduced Cu-SiO_2-AE nanocatalyst. The inset of panel shows the corresponding size distribution diagram.

equation. However, it is worthy to note that there are no obvious diffraction peaks for freshly reduced Cu/SiO_2-AE nanocatalyst except for the diffraction peak at 22 ° for SiO_2 support[39] (Figure S13a), suggesting that the Cu species are highly dispersed on the surface of SiO_2. In addition, there are still no obvious diffraction peaks for Cu/SiO_2-AE nanocatalyst after 120 h evaluation (Figure S13b).

Transmission electron microscopy (TEM) image of calcined Cu/SiO_2-AE sample (Figure 5a) exhibits that the copper phyllosilicate presents lamellar structure, which was formed during the unique ammonia-evaporation process.[39] Figure 5b shows the TEM image of freshly reduced Cu/SiO_2-AE nanocatalyst. The active Cu NPs are homogeneously dispersed on the surface of SiO_2 with the average size of Cu NPs being about 2.1 nm, which is ultrasmall among the reported Cu-based nanocatalysts. The active Cu NPs are still highly dispersed on the surface of SiO_2 after 120 h evaluation (Figure S14), implying the as-synthesized Cu/SiO_2-AE nanocatalyst is quite stable. On the other hand, the Cu NPs of freshly reduced Cu/SiO_2-TI nanocatalyst aggregated and the average size is very large (about 49.5 nm) (Figure S15).

The Cu $2p_{3/2}$ and Cu $2p_{1/2}$ peaks of freshly reduced Cu/SiO_2-AE and Cu/SiO_2-TI nanocatalysts both appear at 932.8 and 952.7 eV, respectively (Figure S16a), which suggests that the Cu^{2+} species in calcined Cu/SiO_2-AE and Cu/SiO_2-TI samples can be both reduced to Cu^+ and/or Cu^0 species.[40] Cu LMM X-ray auger electron spectroscopy (XAES) spectrum is measured to distinguish Cu^+ and Cu^0 species.[41-42] Interestingly, the kinetic energy of Cu/SiO_2-AE nanocatalyst is 914.9 eV, indicating the Cu species is

Table 1. Physicochemical properties of as-synthesized nanocatalysts.

Nanocatalysts	Cu loading (%)	S_{BET}[a] (m^2g^{-1})	D_{Cu}[b] (%)	S_{Cu}[c] (m^2g^{-1})
Cu/SiO_2-AE	10.7	400.7	5.3	31.8
Cu/SiO_2-TI	10.1	335.4	3.1	20.8

[a] S_{BET}: BET surface area of catalysts. [b] D_{Cu}: Cu dispersion of catalysts. [c] Cu specific surface area.

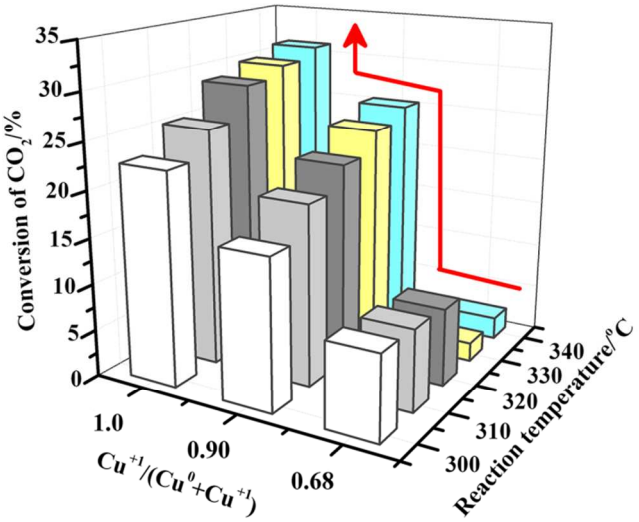

Figure 6. Three-dimensional histogram of conversion of CO_2, $Cu^+/(Cu^o + Cu^+)$ and reaction temperature.

Cu^+, while that of Cu/SiO_2-TI nanocatalyst is 917.6 eV, suggesting the Cu species is Cu^o (Figure S16b).[43, 44] In Figure S17, the dominating Cu species after 120 h of time-on-stream is still Cu^+.

The BET surface area (Table S2, Figure S18 and S19) of Cu/SiO_2-AE nanocatalyst is 400.7 m^2/g, which is higher than that (335.4 m^2/g) of Cu/SiO_2-TI nanocatalyst, suggesting that the AE method is superior to the TI method for acquiring higher BET surface area. Interestingly, there are smaller pores (about 2 nm) distribute in Cu/SiO_2-AE nanocatalyst (Figure S20a), while there are no this kind of pores in Cu/SiO_2-TI nanocatalyst (Figure S20b). The larger BET surface area and small pore size may be benefit for the CO_2 hydrogenation. Moreover, the Cu dispersion (D_{Cu}) and Cu specific surface area (S_{Cu}) of Cu^o in Cu/SiO_2-TI nanocatalyst were measured by N_2O titration, while those of Cu^+ in Cu/SiO_2-AE nanocatalyst were measured by irreversible CO adsorption (Table 1 and Figure S21, see more details in ESI). The D_{Cu} of Cu/SiO_2-AE nanocatalyst is 5.3%, which is higher than 3.1% of Cu/SiO_2-TI nanocatalyst (Table 1). And the S_{Cu} of Cu/SiO_2-AE nanocatalyst is 31.8 m^2/g, which is also bigger than that (20.8 m^2/g) of Cu/SiO_2-TI nanocatalyst. High-angle annular dark-field scanning transmission electron microscopy (HAADF-STEM) and scanning transmission electron microscopy-energy dispersive X-ray (STEM-EDX) were used to determine the surface distribution of Cu^+ species in Cu/SiO_2-AE nanocatalyst (Figure S22 and S23). The relative high D_{Cu} and S_{Cu} could be contributed to the high performance of Cu/SiO_2-AE nanocatalyst.

Three Cu/SiO_2-AE nanocatalysts (Figure S24, see the preparation process in ESI) with the different $Cu^+/(Cu^o + Cu^+)$ ratios have been synthesized to investigate the influence of valence state. The $Cu^+/(Cu^o + Cu^+)$ ratio was determined by Cu LMM XAES spectra (Figure S25 and Figure S26). Notably, the conversion of CO_2 rapidly raises with increasing of the $Cu^+/(Cu^o + Cu^+)$ value and reaches up to the maximum when the $Cu^+/(Cu^o + Cu^+)$ is 1.00, which demonstrates that the Cu^+ species is the active component in Cu/SiO_2-AE nanocatalyst for activation and conversion of CO_2 (Figure 6). Considering the reaction was carried out under reduction atmosphere, we change the reaction temperature of CO2 hydrogenation to 200 °C and maintain other conditions unchanged. The reaction temperature of 200 °C is lower than the reduction temperature (248 °C) obtained from the H_2-TPR profile (Figure S6). It is worth mentioning that the conversion of CO_2 increased significantly with the raising of Cu^+ ratio (Figure S27), which is consistent with the result derived from Figure 6. Therefore, the high ratio of $Cu^+/(Cu^o + Cu^+)$ is mainly responsible for the high performance of Cu/SiO_2-AE nanocatalyst for CO_2 activation.

In summary, we have successfully synthesized a high-performance and long-lived Cu/SiO_2-AE nanocatalyst for CO_2 hydrogenation by ammonia-evaporation method without introducing any structure promoters. The Cu^+ species has been demonstrated to be the active component for the activation and conversion of CO_2. The high value of $Cu^+/(Cu^o + Cu^+)$ is mainly responsible for the high performance of Cu/SiO_2-AE nanocatalyst in CO_2 activation. The ultra-small size, relative high dispersion and specific surface area of Cu^+ species are contributed to the high catalytic activity. The interaction between metal and support mainly accounts for the excellent thermal stability. This work will provide an effiective way for synthesizing transition metal based nanocatalysts (such as Fe, Co, Ni, etc.) with high activity and stability.

ASSOCIATED CONTENT

Supporting Information

Reaction of CO2 hydrogenation to methanol, experimental details, BET surface areas, N_2O titration, irreversible CO adsorption measurement, PXRD patterns, TEM images, HAADF-STEM image, STEM-EDX, XPS and XAES spectra, H_2-TPR profiles, H_2-TGA profile, UV-Vis-NIR diffuse reflectance spectra. This material is available free of charge via the Internet at http://pubs.acs.org.

AUTHOR INFORMATION

Corresponding Author

gcguo@fjirsm.ac.cn (Guo-Cong Guo);
znxu@fjirsm.ac.cn (Zhong-Ning Xu)

Notes

The authors declare no competing financial interest

ACKNOWLEDGMENT.

We gratefully acknowledge financial support from the 973 Program (2011CBA00505, 2013CB933200), the NSF of China (21403237, 21303202, 21303203), the NSF of Fujian Province (2014J05025), and Open Project of State Key Laboratory of Supramolecular Structure and Materials (sklssm201506).

REFERENCES

(1) He, M.; Sun, Y.; Han, B. *Angew. Chem., Int. Ed.* **2013**, 52, 9620–9633.
(2) Mulali, U. A.; Fereidouni, H. G.; Lee, J. Y. M.; Sab, C. N. B. C. *Renewable Sustainable Energy Rev.* **2013**, 23, 107–112.

(3) Dorner, R. W.; Hardy, D. R.; Williams, F. W.; Willauer, H. D. *Energy Environ. Sci.* **2010**, *3*, 884–890.
(4) Doney, S. C.; Fabry, V. J.; Feely, R. A.; Kleypas, J. A. *Annu. Rev. Mar. Sci.* **2009**, *1*, 169–192.
(5) Liu, J.; Li, C.; Wang, F.; He, S.; Chen, H.; Zhao, Y.; Wei, M.; Evans, D. G.; Duan, X. *Catal. Sci. Technol.* **2013**, *3*, 2627–2633.
(6) Falkowski, P.; Scholes, R. J.; Boyle, E.; Canfield, D.; Elser, J.; Gruber, N.; Hibbard, K. *Science* **2000**, *290*, 291–296.
(7) Omae, I. *Coord. Chem. Rev.* **2012**, *256*, 1384–1405.
(8) Razali, N. A. M.; Lee, K. T.; Bhatia, S.; Mohamed, A. R. *Renewable Sustainable Energy Rev.* **2012**, *16*, 4951–4964.
(9) Wang, W.; Wang, S. P.; Ma, X. B.; Gong, J. L. *Chem. Soc. Rev.* **2011**, *40*, 3703–3727.
(10) Preti, D.; Resta, C.; Squarcialupi, S.; Fachinetti, G. *Angew. Chem., Int. Ed.* **2011**, *50*, 12551–12554.
(11) Centi, G.; Quadrelli, E. A.; Perathoner, S. *Energy Environ. Sci.* **2013**, *6*, 1711–1731.
(12) Karelovic, A.; Ruiz, P. *ACS Catal.* **2013**, 3, 2799–2812.
(13) He, S.; Li, C.; Chen, H.; Su, D.; Zhang, B.; Cao, X.; Wang, B.; Wei, M.; Evans, D. G.; Duan, X. *Chem. Mater.* **2013**, *25*, 1040–1046.
(14) Aresta, M.; Dibenedetto, A. *Dalton Trans.* **2007**, 2975-2992.
(15) Baiker, A. *Appl. Organomet. Chem.* **2000**, *14*, 751–762.
(16) Sakakura, T.; Choi, J. C.; Yasuda, H. *Chem. Rev.* **2007**, *107*, 2365–2387.
(17) Appel, A. M.; Bercaw, J. E.; Bocarsly, A. B.; Dobbek, H.; DuBois, D. L.; Dupuis, M.; Ferry, J. G.; Fujita, E.; Hille, R.; Kenis, P. J.; Kerfeld, C. A.; Morris, R. H.; Peden, C. H.; Portis, A. R.; Ragsdale, S. W.; Rauchfuss, T. B.; Reek, J. N.; Seefeldt, L. C.; Thauer, R. K.; Waldrop, G. L. *Chem. Rev.* **2013**, *113*, 6621–6658.
(18) Kleij, A. W. *Catal. Sci. Technol.* **2014**, *4*, 1481–1481.
(19) Meunier, F. C. *Angew. Chem., Int. Ed.* **2011**, *50*, 4053–4054.
(20) Gao, P.; Li, F.; Xiao, F.; Zhao, N.; Sun, N.; Wei, W.; Zhong, L.; Sun, Y. *Catal. Sci. Technol.* **2012**, *2*, 1447–1454.
(21) Arena, F.; Mezzatesta, G.; Zafarana, G.; Trunfio, G.; Frusteri, F.; Spadaro, L. *J. Catal.* **2013**, *300*, 141–151.
(22) Bansode, A.; Urakawa, A. *J. Catal.* **2014**, *309*, 66–70.
(23) Gao, P.; Li, F.; Zhan, H.; Zhao, N.; Xiao, F.; Wei, W.; Zhong, L.; Wang, H.; Sun, Y. *J. Catal.* **2013**, *298*, 51–60.
(24) Liao, F. L.; Huang, Y. Q.; Ge, J. W.; Zheng, W. R.; Tedsree, K.; Collier, P.; Hong, X. L.; Tsang, S. C. *Angew. Chem., Int. Ed.* **2011**, *50*, 2162–2165.
(25) Grabow, L. C.; Mavrikakis, M. *ACS Catal.* **2011**, *1*, 365–384.
(26) Baltes, C.; Vukojevic, S.; Schuth, F. *J. Catal.* **2008**, *258*, 334–344.
(27) Graciani, J.; Mudiyanselage, K.; Xu F.; Baber, A. E.; Rodriguez, J. A., *Science* **2014**, *345*, 546–550.
(28) Reske, R.; Mistry, H.; Behafarid, F.; Cuenya, B. R.; Strasser, P. *J. Am. Chem. Soc.* **2014**, *136*, 6978–6986.
(29) Yue, H.; Zhao, Y.; Zhao, S.; Wang, B.; Ma, X.; Gong, J. *Nat. Commun.* **2013**, *4*, 2339–2346.
(30) Chen, C. S.; Lin, J. H.; You, J. H.; Chen, C. R. *J. Am. Chem. Soc.* **2006**, *128*, 15950–15951.
(31) Zhan, H.; Li, F.; Gao, P.; Zhao, N.; Xiao, F.; Wei, W.; Zhong, L.; Sun, Y. *J. Power Sources* **2014**, *251*, 113–121.
(32) Behrens, M.; Studt, F.; Kasatkin, I.; Kühl, S.; Hävecker, M.; Abild-Pedersen, F.; Zander, S.; Girgsdies, F.; Kurr, P.; Kniep, B. L.; Tovar, M.; Fischer, R. W.; Nørskov, J. K.; Schlögl, R. *Science* **2012**, *336*, 893–897.
(33) Behrens, M., Zander, S., Kurr, P, Jacobsen, N., Senker, J., Koch, G., Ressler T., Fischer, R. W., Schlögl, R. *J. Am. Chem. Soc.* ***2013***, *135, 6061–6068*.
(34) Chen, C. S.; Cheng, W. H.; Lin, S. S. *Chem. Commun.* **2001**, 18, 1770–1771.
(35) Robbins, J. L.; Iglesia, E.; Kelkar, C. P.; DeRites, B. *Catal. Lett.* **1991**, *10*, 1–10.
(36) Lin, J. D.; Zhao, X. Q.; Cui, Y. H.; Zhang, H. B.; Liao, D. W. *Chem. Commun.* **2012**, *48*, 1177–1179.
(37) Behrens, M., Schlögl, R. *Z. Anorg. Allg. Chem.* **2013**, 639, 2683–2695.
(38) Gong, J.; Yue, H.; Zhao, Y.; Zhao, S.; Zhao, L.; Lv, J.; Wang, S.; Ma, X. *J. Am. Chem. Soc.* **2012**, *134*, 13922–13925.
(39) Zheng, X.; Lin, H.; Zheng, J.; Duan, X.; Yuan, Y. *ACS Catal.* **2013**, *3*, 2738–2749.
(40) Chen, L. F.; Guo, P. J.; Qiao, M. H.; Yan, S. R.; Li, H. X.; Shen, W.; Xu, L. H.; Fan, K. N. *J. Catal.* **2008**, *257*, 172–180.
(41) Yue, H.; Ma, X.; Gong, J. *Acc. Chem. Res.* **2014**, *47*, 1483–1492.
(42) Yin, A. Y.; Guo, X. Y.; Fan, K. N. Dai, W. L. *ChemCatChem* **2010**, *2*, 206–213.
(43) Huang, Y.; Ariga, H.; Zheng, X.; Duan, X.; Takakusagi, S.; Asakura, K.; Yuan, Y. *J. Catal.* **2013**, *307*, 74–83.
(44) Yin, A. Y., Guo, X. Y., Dai, W. L., Fan, K. N. *J. Phys. Chem. C* **2009**, 113, 11003–11013.

Table of Contents